M. Kruger and A. Uranga, "The Feasibility of Electric Propulsion for Commuter Aircraft", AIAA 2020-1499, *AIAA Scitech, Orlando, FL, Jan 6-10, 2020.* doi: 10.2514/6.2020-1499

# The Feasibility of Electric Propulsion for Commuter Aircraft

Michael Kruger* and Alejandra Uranga†

*University of Southern California, Los Angeles, CA 90089, U.S.A.*

**The current work presents a sizing and optimization framework that uses a power-based analysis to model transport aircraft with varying degrees of electrification. This framework uses a unified propulsion system model that represents the wide variety of conventional and electrified propulsion system architectures through just one source and one load electrification parameter. The framework is applied to a commuter mission for aircraft carrying up to 19 passengers, and the effects of electrification analyzed based on on-board energy requirements with three different levels of electrical component technology. Results show that energy usage benefits of electrification depend strongly on the assumed technology levels. With today's state-of-the-art batteries and electrical components, electrification is unlikely to prove beneficial. However, with significant technological improvements–in particular for batteries–electrification could substantially reduce energy needs. For a 463 km (250 nmi) mission, an all-electric architecture reduces energy consumption by up to 69% based on our optimistic 2035 technology assumptions. Hybrid-electric configurations can retain a significant proportion of the benefit while increasing the feasible mission range: for an extended range of 926 km (500 nmi), an aircraft storing 90% of its energy in batteries and 10% in fuel could reduce energy consumption by as much as 63% for the optimistic technology assumptions, and as much as 27% with more realistic 2035 technology values. Furthermore, we find that technologies enabled by electrification, specifically distributed propulsion and boundary layer ingestion, could play an important role in facilitating electrification, although to a lesser degree than the other technological advances.**

## I. Introduction

Recent studies show that adopting an electrified propulsion system for commercial aircraft has potential advantages in terms of the energy required to perform certain missions relative to conventionally powered aircraft [1–5]. However, these studies have been limited to considering only one particular propulsion system architecture at a time, and/or have looked at the trade-offs of the design space with only low fidelity models.

The present work introduces a framework to size and optimize aircraft for a variety of missions (payload and range) using a broad range of propulsion system architectures, from conventional turboprop and turbofan engines, to hybrid-, turbo- and all-electric propulsion. A unified propulsion system model is used in order to represent the wide variety of propulsion system architectures via just two electrification parameters. The framework also models the effects of boundary layer ingestion (BLI) and of distributed propulsion (DP). These models are implemented into the Stanford University Aerospace Vehicle Environment (SUAVE) [6] for mission analysis and the PyOptSparse package [7] as a wrapper for aircraft sizing and optimization. The goal is to conduct trade-space studies at a level of fidelity that will allow us to determine which architectures are best—in terms of on-board energy usage–for which missions with a low degree of uncertainty.

Our framework is applied to the exploration of the design space for aircraft belonging to the commuter category, designed to carry up to 19 passengers. Three different technology levels (as defined via values for battery specific energy, component efficiencies and specific powers) are adopted, and the framework is validated against a conventional baseline aircraft. With the mission-specific on-board energy usage as performance metric, the effects of electrification, boundary layer ingestion, and distributed propulsion are studied.

In this work, we define the *electrification level* via the two parameters in the unified propulsion system model: the splits in power at the level of the energy sources (turbo-generators and/or batteries) and load (propulsive power from mechanically-driven and/or electrically-driven fans). The term *electrification design space* refers to the possible combinations of propulsion system architectures.

*Graduate Student, Dept. of Aerospace and Mechanical Engineering, AIAA Student Member

†Gabilan Assistant Professor, Dept. of Aerospace and Mechanical Engineering, 854 Downey Way RRB 218, auranga@usc.edu, AIAA Senior Member

The paper first presents the framework methodology in detail. We start with the unified propulsion system model and the aircraft-level power accounting, before describing the mission analysis integration for sizing and optimization. The framework is then applied to a commuter aircraft mission.

## II. Modeling

### A. Unified Model of Propulsion Architectures

A propulsion system model was presented in a previous work [1] that is capable of modeling various types of propulsion system architectures by simply changing some model parameters. This *unified model* can model various fundamentally different propulsion systems, from conventional (internal combustion) systems to hybrid-electric, turbo-electric and all-electric. A schematic diagram of the unified model is shown in Fig. 1.

The unified model is completely general and can be implemented in any aircraft analysis program. For the purpose of the current work, it was implemented in SUAVE and used along the mission to determine the power used by every component. Knowing the power required by all components allows for the fuel consumed by the gas turbine/s (if present) and the power drawn from the battery (if present) to be computed. Given peak power requirements, the unified model can also be used to determine the maximum power used by each component at some point in the mission, which can then be used to size the component. The flexibility of this model allows for different *electrification schemes* to be used along the mission, while sizing the components to ensure that they can provide adequate power throughout the mission. An example of one electrification scheme might be using battery power during takeoff and climb only, which provides a power boost and allows the gas turbine to be sized for cruise conditions, possibly leading to a lighter, more efficient aircraft.

This model sees the propulsion system as having two different air streams for adding power to the flow, which in a traditional framework can be seen as providing a given thrust. One stream is from mechanically powered fans and the other from electrically powered fans. These air streams can be from one or many individual propulsors.

Electrification of the propulsion system can be defined based on the two distinct parameters

$$f_L \equiv \frac{P_{K,E}}{P_{K,E} + P_{K,M}} \tag{1}$$

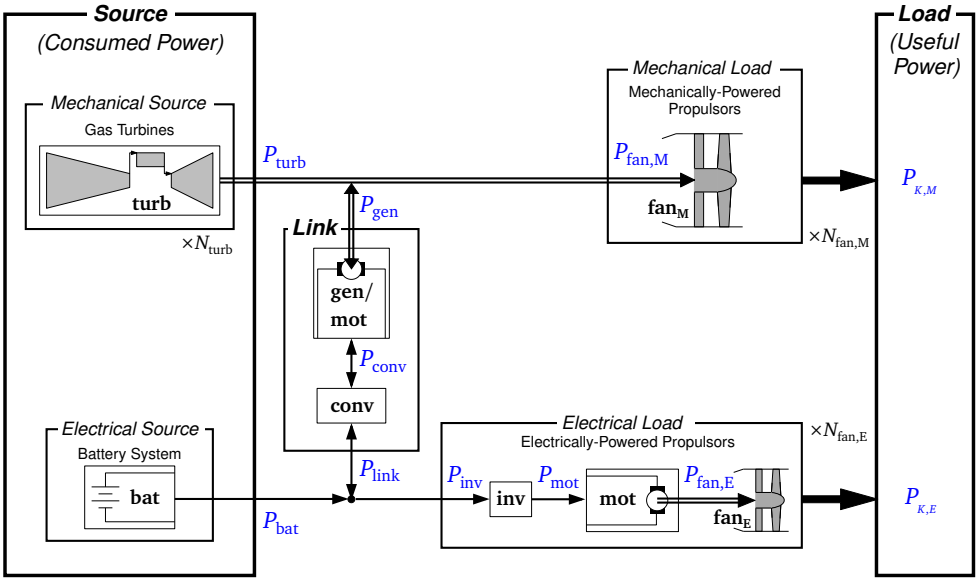


**Fig. 1 Unified propulsion system model [1]. The subscripts M and E refer to mechanical and electrical components, respectively, and the powers $P$ indicate the power flow between components.**

and

$$f_S \equiv \frac{P_{\text{bat}}}{P_{\text{bat}} + P_{\text{turb}}} . \tag{2}$$

The load electrification factor, $f_L$, defines the split between flow power coming from the electrical and mechanical propulsive streams, $P_{K,E}$ and $P_{K,M}$, respectively. The source electrification factor, $f_S$, defines the split between power coming from a chemical battery and a gas-powered turbine, $P_{\text{bat}}$ and $P_{\text{turb}}$, respectively. The mechanical and electrical subsystems can be connected with an energy conversion device that could either function as a motor or as a generator, depending on the direction of flow in the link between the two systems. If the power flows from the upper to the lower system in Fig. 1, the link is a generator. In this case the system could be either series hybrid- or turbo-electric. Conversely, if the power flows upwards the link is a motor and the system is parallel hybrid. A choice of $f_S$ and $f_L$ defines a unique propulsion system, and in this way the unified model can be used to model any of the distinctly different systems mentioned above. If the total required flow powers ($P_{K,M} + P_{K,E}$) are known, together with a specified $f_S$ and $f_L$, the power required by each component in the propulsion system can be uniquely determined. These component powers are then used to size the components based on the maximum power they require along the mission, and they are also used to determine the fuel and battery power, and thus energy required This directly determines the fuel and battery masses required to perform a given mission.

Figure 2 shows the design space as defined by different $f_S$ and $f_L$ combinations. As $f_S$ increases, the fraction of source power provided by the battery increases, and as $f_L$ increases, the fraction of load power provided by electrically powered fans increases. The dashed line running through the center corresponds to the point where the power flowing in the link connecting the mechanical and electrical subsystems is zero, and the two subsystems essentially act independently. Below this line, the configuration is a *parallel hybrid*, and the link acts as a motor. Here, the battery provides a power boost to the mechanically powered propulsors. Above this line, the configuration is a *series hybrid*, and the link acts as a generator. Here, the battery power is supplemented by power generated by the link, which is coupled to the gas turbine(s). The left vertical axis ($f_S = 0$, $0 < f_L < 1$) represents *partial turbo-electric* configurations, with all energy stored in fuel, but flow power being provided by a split between conventionally powered propulsors, and electric motors being powered by the link generator/s coupled to turbofan output shafts. For the *fully turbo-electric* case ($f_S = 0$, $f_L = 1$), all power is provided by electrically powered fans, and the power source is a pure turbo-generator, not producing any thrust. Note that the right boundary ($f_S = 1$,$0 \leq f_L < 1$) represents a non-physical boundary where all source power comes from a battery, but this power cannot, by definition, be used to power mechanical propulsors. The two opposing corners of the design space ($f_S = f_L = 0$ and $f_S = f_L = 1$) represent purely *conventional* and *all-electric* configurations respectively.

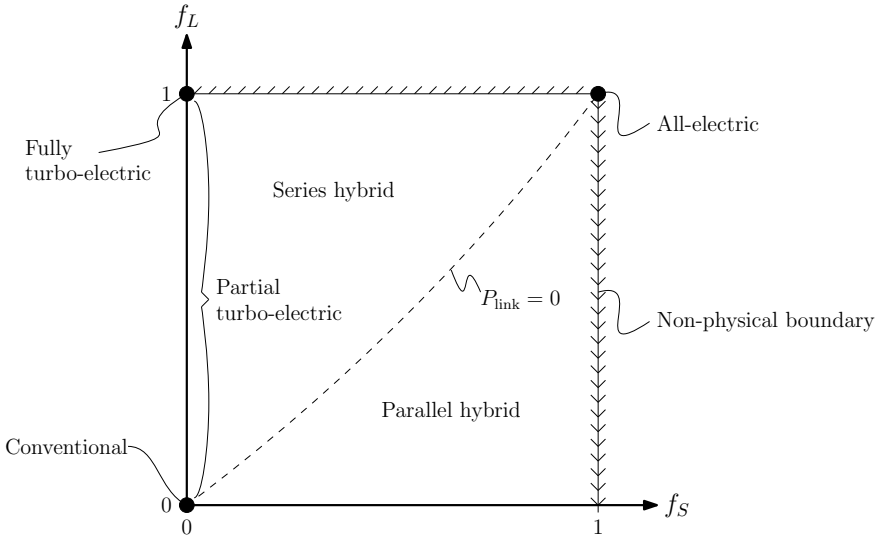


**Fig. 2 Schematic of $f_S$-$f_L$ design space.**

The direction of the flow in the link is a function of $f_L$, $f_S$ and the link electrical machine and power electronics efficiencies $\eta_{\text{EM}}$ and $\eta_{\text{PE}}$. The flow in the link is upwards (link as motor) if

$$(1 - f_S) f_L < \eta_{\text{EM}}\, \eta_{\text{PE}}\, f_S (1 - f_L) , \tag{3}$$

and downwards (link as generator) if

$$(1 - f_S) f_L > \eta_{\text{EM}}\, \eta_{\text{PE}}\, f_S (1 - f_L)\,. \tag{4}$$

In the case that Equation 3 holds,the unified model can be described with the system of equations

$$\begin{aligned}
P_{K,M} &= (1 - f_L) P_{K,\text{tot}} \\
P_{K,E} &= f_L P_{K,\text{tot}} \\
P_{\text{fan,M}} &= \frac{P_{K,M}}{\eta_{\text{fan}}} \\
P_{\text{fan,E}} &= \frac{P_{K,E}}{\eta_{\text{fan}}} \\
P_{\text{mot}} &= \frac{P_{\text{fan,E}}}{\eta_{\text{EM}}} \\
P_{\text{inv}} &= \frac{P_{\text{mot}}}{\eta_{\text{PE}}} \\
P_{\text{bat}} &= P_{\text{inv}} + P_{\text{link}} \\
P_{\text{bat}} &= \frac{f_S}{1 - f_S} P_{\text{turb}} \\
P_{\text{turb}} &= P_{\text{fan,M}} - \eta_{\text{EM}} \eta_{\text{PE}} P_{\text{link}}
\end{aligned} \tag{5}$$

In the case that Equation 4 holds, the last equation in system 5 should be replaced with

$$P_{\text{turb}} = P_{\text{fan,M}} - \frac{P_{\text{link}}}{\eta_{\text{EM}} \eta_{\text{PE}}}\,. \tag{6}$$

The nomenclature used here is the same as that from Fig. 1, and the subscripts EM and PE stand for *electrical machine* (motors, generators) and *power electronics* (rectifiers, inverters and associated controllers), respectively.

For a specified $f_L$, $f_S$, component efficiencies $\eta_{\text{comp}}$ and a total required flow power $P_{K,\text{tot}}$ these equations represent a linear system that can be solved for the individual component powers. When cast into matrix form, these systems can be solved numerically using any linear algebra subroutine. This system is shown in matrix form in the Appendix.

It is emphasized that the power flow through the system as described here represents an instantaneous snapshot of the system, and the power flow can vary over time. For instance, as the aircraft weight deceases, less power is required. Also, the power flow could be completely different for different mission segments, depending on the *electrification strategy* used. For instance, to take advantage of more degrees of freedom in the propulsion system architecture, some components might only be used during some mission segments.

### B. Propulsion System Sizing and Distribution

The weights of the propulsion system components are calculated either as a function of the maximum power level they are required to operate at during some point along the mission, or their physical size, as is the case for the fan nacelles. The overall propulsion system mass is equal to the sum of its component masses, such that

$$\begin{aligned}
m_{\text{prop}} &= N_{\text{fan,M}} \left( m_{\text{EM,link}} + m_{\text{PE,link}} + m_{\text{turb}} + m_{\text{fan,M}} + m_{\text{nace,M}} \right) \\
&\quad + N_{\text{fan,E}} \left( m_{\text{inv}} + m_{\text{mot}} + m_{\text{fan,E}} + m_{\text{nace,E}} \right) \\
&\quad + m_{\text{TMS}}\,.
\end{aligned} \tag{7}$$

The masses of the turbine cores are calculated as [8]

$$m_{\text{turb}} = 1.67 P_{\text{turb}}^{0.803}\,, \tag{8}$$

where $P_{\text{turb}}$ should be specified in hp and the resulting mass is in lbs. The different propulsors modeled in the framework are either mechanically powered fans or propellers, or electrically powered fans.

If the engine is a turboprop engine, the propeller mass is calculated as [9]

$$m_{\text{propeller}} = 0.108 \left( D_{\text{propeller}} P_{\text{propeller}} \sqrt{N_{\text{blades}}} \right)^{0.78174}\,, \tag{9}$$

where diameter $D$ is specified in ft and power $P$ in hp, and the resulting mass is in lbs. Here $N_{\text{blades}}$ is the number of blades on the propeller.

If the propulsors are either mechanically powered fans, such as turbofan fans, or electrically powered fans, the fan masses are calculated per [10] as

$$m_{\text{fan,M/E}} = 0.290\dot{m}^{1.143} \,, \tag{10}$$

where $\dot{m}$ is the mass flow through the fan in lbs/s.

The electrical machines and power electronics are assumed to have constant specific powers, so their masses are determined from an assumed power-to-mass ratio $\left[\frac{P}{m}\right]$ as

$$m_{\text{comp}} = P_{\text{comp}} \left[\frac{P}{m}\right]^{-1}_{\text{comp}} \,, \tag{11}$$

where 'comp' denotes the specific component the equation is applied to. The total nacelle mass is calculated per [8] as

$$m_{\text{nac,M/E}} = 0.6724\, K_{\text{ng}} \ell_{\text{nac}}^{0.10} D_{\text{nac}}^{0.294} N_z^{0.119} m_{\text{eng}}^{0.661} S_n^{0.224} \,. \tag{12}$$

Input units must be in English units and the result is given in lbs. Here $K_{\text{ng}}$ is 1.017 for a pylon-mounted nacelle, and 1.0 otherwise, $\ell_{\text{nac}}$ and $D_{\text{nac}}$ are the nacelle length and width, respectively, in feet, $N_z$ is the ultimate load factor (1.5 times limit load factor), $m_{\text{eng}}$ is the mass of the engine or motor inside the nacelle in lbs and $S_{\text{nac}}$ is the nacelle wetted area in square feet.

In the case of a turboprop engine, the core dimensions are estimated as [8]

$$D_{\text{core}} = 0.25(P_{\text{turb}}/1000)^{0.120} \,, \tag{13}$$

$$\ell_{\text{core}} = 0.12(P_{\text{turb}}/1000)^{0.373} \,, \tag{14}$$

with $P_{\text{turb}}$ in kW. The turboprop nacelle diameter is then estimated as $1.2D_{\text{core}}$. The nacelle mass is then also calculated using Equation 12. The core can, however be specified to be housed internally in the fuselage, as in the case that it only acts as a generator, in which case it does not have a nacelle which does thus not contribute to weight or drag.

The model also accounts for the weight of a thermal management system which is used to remove waste heat from all the electrical components. The mass of this system scales with the heat flow, again via a power-to-mass ratio, so its mass is

$$m_{\text{TMS}} = \dot{Q} \left[\frac{P}{m}\right]^{-1}_{\text{TMS}} \,, \tag{15}$$

where $\dot{Q}$ is the total waste heat from all electrical components, computed as

$$\dot{Q} = \sum_{\text{i}}^{N_{\text{comp}}} (1 - \eta_{\text{i}}) P_{\text{i}} \,. \tag{16}$$

It is assumed that the electrically powered fans are embedded in the wings and their nacelles have only half the surface area of the mechanically powered propulsors, which are podded and fully immersed in the free stream. An electrical propulsor nacelle having a similar diameter as a mechanical one will thus weigh less than the mechanically powered one, and experience less drag. If the conventional engine is a turboprop, it is assumed to be mounted directly to the wing and does thus not have a pylon. If they are podded engines such as turbofans, it is assumed that the mechanical propulsors are pylon-mounted. In either case, the value of $K_{\text{ng}}$ in Equation 12 is set appropriately. The electrically powered fans are assumed to be embedded over the trailing edge of the wing. It was found by [11] that this location is most beneficial for distributing multiple propulsors over the wing. Equation 12 is thus evaluated separately for the mechanical and electrical propulsors. Figure 3 schematically shows how the electrical propulsors are sized to maximize distribution and BLI potential. The total electrical propulsor mass flow and propulsive area is divided equally among the propulsors shown here.

More formally, the amount of boundary layer ingested refers to the fraction of total airframe momentum defect in the boundary layer that is ingested and re-energized. The total aircraft viscous or profile drag is a function of this momentum defect [12] and the amount of BLI can thus be estimated via viscous drag arguments. It is assumed that roughly 50% of the total viscous drag is caused by the wing, which is a reasonable estimate for tube-and-wing

configurations. Furthermore, it can be demonstrated via airfoil/wing boundary layer theory that roughly 80% of the wing momentum defect occurs on the top surface due to the higher surface speeds and thus higher velocity gradients seen there [12]. The total fraction of ingestible wing momentum defect is thus taken as $f_{MD} = 0.4$. To avoid integration difficulties, it is assumed that the fuselage diameter is excluded from the wing span $b$, and that 80% of the remaining span is available for distributing propulsors, leaving 20% free for control surfaces that might not be compatible with embedded trailing edge propulsors. The total fraction of BLI due to the electrical propulsors is thus given as

$$f_{\mathrm{BLI,E}} = f_{MD} \frac{N_{\mathrm{fan,E}} \times D_{\mathrm{nac,E}}}{b - d_{\mathrm{fuse}}} \,. \tag{17}$$

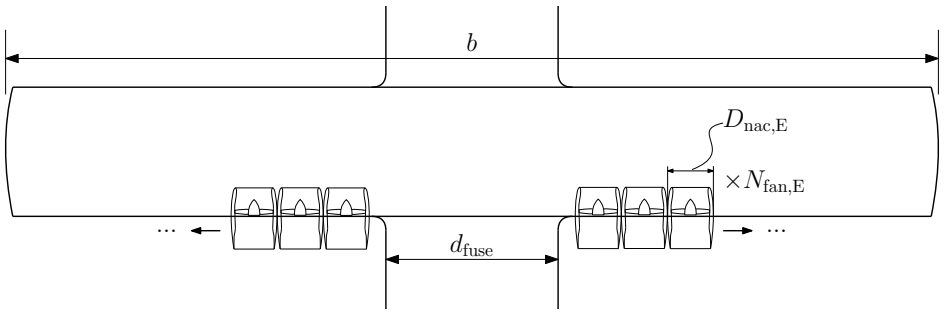


**Fig. 3 Electrical propulsors sizing and distribution.**

### C. Power Accounting and BLI

Electrification is seen as an enabling technology for distributed propulsion (DP) and boundary layer ingestion (BLI). A goal for the current framework is the analysis of aircraft making extensive use of these technologies and there are thus strong interactions between the aircraft aerodynamics and the propulsion system. For aircraft with BLI the distinction between thrust and drag is not well defined, and the power balance method [13] is used here to avoid this problem. The power balance method formulates the aero-propulsive problem based on power and dissipation rather than thrust and drag, since power and dissipation are both clearly defined for aircraft ingesting significant fractions of their boundary layers. Various papers have been published that use the power balance method to model the aero-propulsive interactions of aircraft [14, 15].

The flow power added to a propulsive stream, $P_K$, is given by [15]

$$P_K = \frac{1}{2}(V_{\mathrm{jet}}^2 - V_\infty^2)\dot{m} + f_{\mathrm{BLI}}\, f_{\mathrm{surf}}\, D'_p\, V_\infty \,, \tag{18}$$

where $V_{\mathrm{jet}}$ is the propulsive jet velocity, $V_\infty$ is the freestream velocity, $\dot{m}$ is the total mass flow through the propulsor, $f_{\mathrm{BLI}}$ is the fraction of the total momentum defect ingested and re-energized by the BLI propulsors, $f_{\mathrm{surf}}$ is the fraction of total dissipation occurring on the aircraft surface, as opposed to in the wake, and $D'_p$ is the total viscous (or profile) drag acting on an equivalent non-BLI aircraft. For more detailed definitions of the variables used here, the original source should be consulted [15].

The net stream-wise force acting on the aircraft, $F_X$,is given by

$$F_X = D' - f_{\mathrm{BLI}} D'_p - \Delta\Phi_{\mathrm{surf}}/V_\infty - (V_{\mathrm{jet}} - V_\infty)\dot{m} + \dot{h}\,\frac{W}{V_\infty} \,. \tag{19}$$

Here $D'$ is the total drag force experienced by an equivalent non-BLI aircraft, $\Delta\Phi_{\mathrm{surf}}$ is the change in surface dissipation due to the installation of the BLI propulsors, $\dot{h}$ is the rate of climb and $W$ is the aircraft weight. Note that for steady flight, $F_X$ is zero.

The propulsive efficiency of the aircraft can be calculated as

$$\eta_{\mathrm{prop}} = \frac{P_K - \Phi_{\mathrm{jet}}}{P_K} \,, \tag{20}$$

where $\Phi_{jet}$ is the total dissipation occurring in the jet wake, given by

$$\Phi_{jet} = 1/2(V_{jet} - V_\infty)^2 \dot{m} \ . \tag{21}$$

The last equation required to close the system of power balance equations relates the jet area with the mass flow. This equation requires an assumption of the contraction of the propulsive jet from the propulsor nozzle plane to the downstream value when the jet pressure has returned to the freestream value. Based on published numerical data [15], a 60% contraction is assumed in the current work, giving

$$A_{jet} = 0.6 \times \frac{\dot{m}}{\rho_\infty V_{jet}} \ . \tag{22}$$

In the current work, where an aircraft can be modeled as having multiple propulsors and thus multiple propulsive streams, the propulsive streams are combined by summing the total propulsive areas and mass flows to solve the equations given above. This results in an overall equivalent jet velocity and propulsive efficiency for the aircraft. Equations 18-22 are assembled into a system of equations, and solved numerically.

### D. Drag/Dissipation Buildup

For an aircraft with no BLI, the surface dissipation is directly related to the viscous drag acting on its surface. The dissipation can thus be calculated using a standard friction and form drag (often called parasite drag) buildup, such as is presented in Raymer [8]. Such a method is already implemented in SUAVE, and it is used as is. The only exception is the drag caused by the propulsors, which is added to the framework as part of this work. For an aircraft with BLI, the surface dissipation can still be estimated in this manner, and the effect of BLI can be modeled using the method that was described in Section II.C.

In the current work, the propulsor drag is calculated using the methods described in Raymer [8]. As mentioned in Section II.B, it is assumed that the mechanically powered propulsors are podded turbofan engines, which are fully immersed in the free stream, or turboprop engines that are attached directly to the wing. The electrically powered propulsors are embedded in the wings such that only half of their surface area are exposed to the free stream. An electrically powered propulsor will thus experience half the drag (and thus, dissipation) of a mechanically powered one with a similar fan diameter. Note that this assumption might underestimate drag for large propulsors that cannot be fully integrated into the wing, but should be a reasonable estimate for a large number of small-diameter fans. In fact, this assumption might even be conservative, since it is likely that the total wetted surface of such an integrated array of propulsors could be made less than the sum of the surface areas of the individual propulsors.

## III. Integration Framework

### A. Mission Analysis

The Stanford University Aerospace Vehicle Environment (SUAVE) is used in the current work for the purpose of mission analysis. It has built-in analysis models for aerodynamics, structures and performance. These models can be used as is, extended, or changed for any user-defined model. There are also standard component models for wings, fuselages, propulsion systems and landing gear, which are used by the analysis models to determine aircraft performance. In the current work, the built-in SUAVE models for the wings (main and tail), fuselage, landing gear and other non-structural components are used, but custom models for propulsion system weight and performance are implemented. These models were discussed in Section II. In the current work, only some features of SUAVE will be discussed, since it is thoroughly documented elsewhere [6].

Traditionally, mission analysis programs integrate the equations of motion of the aircraft along a specified mission to determine integrated quantities such as fuel burn. SUAVE takes a different approach by defining all parameters that vary over a mission as Chebyshev polynomials and modeling the mission as a system of equations. An array of unknown mission parameters is created with a user specified number of control points along the mission, and a root finding algorithm is used to solve for the unknowns. This approach has the benefit that any amount of unknown parameters can be added to the system, as long as the system is still determinate, and the mission solver can solve for them without any changes in the solution routine. This extensibility makes SUAVE very suitable for modeling aircraft with complex propulsion systems, or *energy networks* in the SUAVE nomenclature.

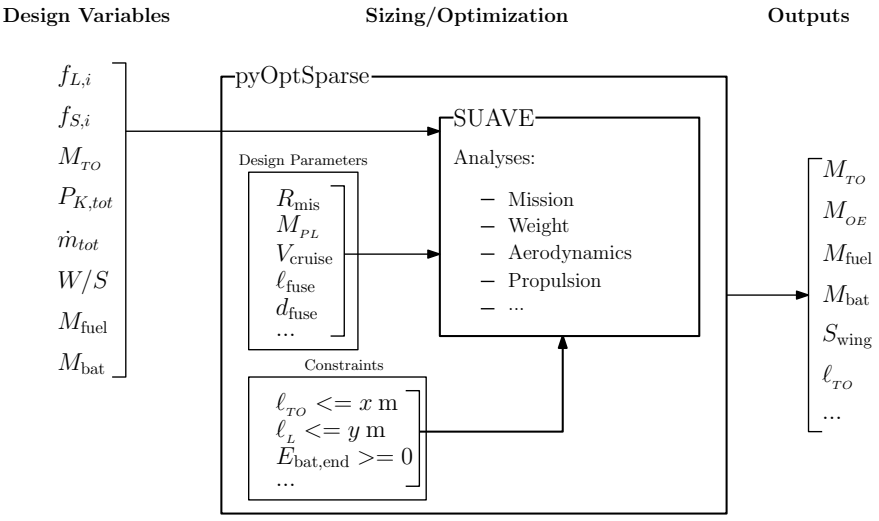


**Fig. 4 Integration of pyOptSparse and SUAVE.**

Various analysis models exist in SUAVE, and the user can define a set of analyses to perform on the aircraft being analyzed. Some analyses, such as aerodynamics and weights, are required for the mission solver to function, whereas others, such as a stability analysis, are optional. Analysis routines can also be coupled by using the outputs of one analysis as the inputs to others. This allows the complex interactions between subsystems to be modeled. A weight analysis model could be as simple as a user specified takeoff weight, or a full structural analysis linked to an external finite element program. An aerodynamics model could be a simple component drag buildup, or a computational fluid dynamics analysis. This interchangeability of component and analysis models and the extensibility of the mission solver allows the user to tailor the fidelity level of the SUAVE analysis to their desired level, and allows them to even use different fidelity levels for different analyses/models.

The above is a very simplified description and the original paper [6] should be consulted for a more thorough description.

### B. Aircraft Sizing and Optimization

The current framework is built around SUAVE and uses the pyOptSparse [7] optimization framework with the SNOPT (Sparse Nonlinear OPTimizer) solver [16] to converge the sizing process and perform optimization. SUAVE is a framework written in Python, which at its core is a mission analysis framework that analyzes a given 'fixed' aircraft, but can be easily wrapped within other code to perform sizing and optimization studies. The implementation of its core functionality is documented in [6], which should be consulted for a detailed description of the workings of SUAVE. SUAVE was designed to be extensible and in the current work, various new models are created and implemented. The main characteristics of these models are that they allow for the analysis of complex propulsion systems that are, at the time of writing, not available in SUAVE.

In order to perform optimization studies, an optimization wrapper was created by the SUAVE developers that can use various frameworks to perform the actual optimization, as documented in [17]. Various different optimizers were compared in [18] and those researchers found that SNOPT (as described below) gave the best overall results.

In the current framework the wrapper created for pyOptSparse was used. pyOptSparse is a constrained non-linear optimization framework that was developed from pyOpt [7], with sparse matrices used throughout the code. pyOptSparse is capable of using various existing optimization solvers, and here SNOPT is used. SNOPT is a Fortran library that is especially effective in optimizing functions with cost functions that are computationally expensive to evaluate, and is thus well-suited for aircraft multi-disciplinary design and optimization problems.

Figure 4 shows schematically how SUAVE and pyOptSparse are integrated in the current framework. SUAVE is used to analyze a given aircraft and contains modules for mission, weight, aerodynamics, propulsion and stability analyses, to name a few. Analyses can be added on in a modular sense, for e.g. if the user is not interested in stability information, this analysis module can be deactivated. New analyses can also be added to SUAVE.

SUAVE can in some sense be used as a 'black box' that takes various aircraft input parameters, and gives various

outputs based on the mission analysis, although the user has full access to the inner workings of the black box. As an optimization framework through the pyOptSparse wrapper, the user can decide which parameters should be optimized and which ones should be fixed. The user supplies bounds for all the *design variables*, as well as constraints and scaling values for the variables and constraints. Examples of design variables to be optimized in the current work are electrification levels $f_{L,i}$, $f_{S,i}$ and wing loading wing loading $W/L$. Here, the subscripts $i$ denote that electrification level can vary between different mission segments. *Design parameters* that are kept fixed during sizing and optimization might include fuselage length and width: $\ell_{\text{fuse}}$, $d_{\text{fuse}}$, mission range $R_{\text{mis}}$, payload mass $M_{PL}$, cruise speed $V_{\text{cruise}}$, and altitude $h_{\text{cruise}}$. Design parameters can be changed to design variables if the user wants to optimize them, although care has to be taken that the model actually contains the required sensitivities to the design variable, otherwise it could lead to numerical issues and the 'optimized' value of the variable might not be physically correct.

Given a set of design variables, design parameters, and constraints, SUAVE performs a user-specified flight mission. In the current work, the mission consists of a climb, cruise and descent segment, as well as a reserve cruise segment. The detailed mission profile flown will be presented later. SUAVE then returns various outputs to pyOptSparse that iterates the design in order to minimize a cost function while ensuring all constraints are met. In this framework, sizing is performed using an *optimizer decomposition* approach with *compatibility constraints* of the form $y = y'$, as presented by Kroo [19]. Here the variable $y$ is the design variable, and $y'$ is the actual value of the variable calculated in the framework. Using this approach the aircraft sizing equations are written as a set of constraints of the form $y/y' = 1 \pm \epsilon$, where $\epsilon$ is a user specified tolerance.

In the current work, sizing variables are takeoff mass $M_{TO}$, total propulsor mass flow $\dot{m}_{\text{tot}}$, fuel mass $M_{\text{fuel}}$, battery mass $M_{\text{bat}}$, and total flow power $P_{K,\text{tot}}$. Note that in the optimizer decomposition method, the optimizer itself makes no distinction between the sizing constraints discussed here and the performance constraints that will be presented next, Both sets of constraints are enforced simultaneously.

### C. Performance Constraints

In order to ensure that the aircraft can meet certain performance requirements, the following performance constraints are implemented. A maximum takeoff field length constraint is implemented using the methods given by Raymer [8] as

$$\ell_{\text{TO}} \leq \ell_{\text{G}} + \ell_{\text{T}} + \ell_{\text{C}} \,, \tag{23}$$

where $\ell_{\text{G/T/C}}$ represent the ground distances covered during the ground roll, transition and obstacle clearance segments of the takeoff segment, respectively. A maximum landing field length constraint is implemented, also using the methods from Raymer as

$$\ell_{\text{L}} \leq \ell_{\text{A}} + \ell_{\text{F}} + \ell_{\text{G}} \,, \tag{24}$$

where $\ell_{\text{A/F/G}}$ represent the ground distances covered during the approach, flare and ground roll segments of the landing segment, respectively. The equations used to estimate these segment lengths can be found in Raymer [8].

To ensure the aircraft has enough power to meet a specified maximum climb rate, the thrust-to-weight ratio is first calculated as

$$(T/W)_{\text{climb}} = \frac{1}{C_L/C_D} + \frac{\text{ROC}}{V_\infty} \,, \tag{25}$$

where ROC is the specified rate of climb. The power constraint is then written as

$$P_{K,\text{tot}} \geq (T/W)_{\text{climb}} \, M_{TO} V_\infty \, g \,, \tag{26}$$

where $g$ is the acceleration due to gravity.

It is assumed that fuel is stored in the aircraft wing and that batteries can be stored either in the wing or in the fuselage. 50% of the wing volume is allocated for fuel or battery storage (a conservative estimate compared to guidelines given in [9] and [8]). An additional 5% of fuselage volume is also allocated for battery storage. The wing volume is estimated as [20]

$$V_{\text{wing}} = \frac{k_Q r}{\sqrt{1+\lambda}} \, S \sqrt{\frac{S_w}{AR}} \,, \tag{27}$$

where $r$ is the ratio of wing frontal to planform area, $\lambda$ is the wing taper ratio, $S_w$ is the wing planform area and $AR$ the aspect ration, and a typical value for $k_Q$ is 0.95 [20]. The fuselage volume is estimated as [20]

$$V_{\text{fuse}} = S_f \times (\ell_{\text{fuse}} - 2\, w_{\text{fuse}}) \,, \tag{28}$$

where $S_f$ is the fuselage frontal area, $\ell_{\text{fuse}}$ is the fuselage length and $w_{\text{fuse}}$ the fuselage width (or diameter). The fuel and battery volume constraints are then given as

$$V_{\text{fuel}} \leq 0.5\, V_{\text{wing}}\,, \tag{29}$$

$$V_{\text{bat}} \leq 0.05\, V_{\text{fuse}} + (0.5\, V_{\text{wing}} - V_{\text{fuel}})\,. \tag{30}$$

In order to ensure the wing is of adequate size, wing loading constraints are implemented to ensure adequate stall and approach speeds. The stall speed is estimated from an assumed maximum aircraft lift coefficient as [8]

$$V_{\text{stall}} = \sqrt{\frac{2M_{TO}\, g \rho_{\text{SL}}}{\rho S_w C_{L,max}}}\,, \tag{31}$$

where $\rho_{SL}$ is sea level air density, $\rho$ is the air density at the altitude where the equation is evaluated, $S_w$ is the wing planform area and $C_{L,max}$ is the wing maximum lift coefficient. The approach speed is taken as 1.22 times the stall speed [20] calculated at landing weight:

$$V_{\text{app}} = 1.22 \sqrt{\frac{2\,(M_{TO} - M_{\text{fuel}})\, g\, \rho_{\text{SL}}}{\rho\, S_w\, C_{L,max}}}\,. \tag{32}$$

The wing loading constraint for stall speed is then

$$W/S|_{\text{stall}} \leq \frac{1}{2}\, \rho_{\text{SL}} V_{\text{stall}}^2 C_{L,max}\,, \tag{33}$$

and for approach it is [20]

$$W/S|_{\text{app}} \leq 0.335\, \rho_{\text{SL}} V_{\text{app}}^2 C_{L,max}\,. \tag{34}$$

The wing loading constraints are evaluated at sea level conditions, so $\rho$ in Equations 31 and 32 are substituted with $\rho_{\text{SL}}$. Furthermore, the specific values assumed for the various performance constraints in this work will be presented in the following section.

## IV. Application: Commuter Aircraft

### A. Performance Metric

In order to compare different aircraft concepts across various missions, the performance metric selected for this work is the *Productivity Specific Energy Consumption*, defined as the energy used during flight divided by the product of payload weight and range, namely

$$PSEC \;\equiv\; \frac{[\text{On board energy}]}{[\text{Payload weight}] \times [\text{Range}]}\,. \tag{35}$$

This metric is comparable to the liters of fuel consumed per passenger-kilometer (or gallons per seat-mile) that is typically used as a measure of the efficiency of transport aircraft. Being more general, however, $PSEC$ allows for the comparison of aircraft with different energy storage sources, such as hydrocarbon fuel and/or batteries. It has also the advantage of being dimensionless. All sizing and Optimization studies performed in the current work use $PSEC$ as the cost (merit) function.

It should be noted that the present work considers only *on board* energy consumption, rather than including a full 'well-to-wake' analysis. As such, any consideration related to the energy used to produce jet fuel or charge batteries before flight is beyond the scope of this work.

### B. Electrical Technology Level Assumptions

The modeling of electrified aircraft in our framework requires as input some parameters for electrical components that are dependent on an assumed technology level. Examples of such parameters are the specific energies and/or powers of the components used in the propulsion system, as well as their efficiencies. The values given to these parameters are referred to as *technology level*.

**Table 1 Technology level parameters for 2035 time frame [1].**

| Parameter | | Conservative | Intermediate | Optimistic |
|---|---|---|---|---|
| Pack-level battery specific energy | [W·h/kg] | 250 | 575 | 900[a] |
| Pack-level battery specific power | [kW/kg] | 0.745 | 1.7 | 2.7 |
| Electrical machine specific power | [kW/kg] | 9 | 12 | 16 |
| Power electronics specific power | [kW/kg] | 9 | 14 | 19 |
| Thermal management system specific power | [kW/kg] | 13.2 | 13.2 | 13.2 |
| Electrical component efficiencies | [-] | 0.98 | 0.99 | 0.99 |

[a]Value is estimated as the geometric mean of the fully charged and fully discharged states of the predicted specific energy of Lithium-Air battery

**Table 2 Characteristics of baseline conventional aircraft.**

| | Viking DHC-6 Series 400 Twin Otter |
|---|---|
| Maximum takeoff mass $M_{TO}$ | 5 670 kg |
| Wing span | 19.81 m |
| Wing loading at $M_{TO}$ | 146 kg/m$^2$ |
| Maximum number of passengers | 19 |
| Design range with 17 passengers | 463 km (250 nmi) |
| Cruise speed | 93.6 m/s (182 kts) |
| Fuselage diameter | 1.83 m |
| Fuselage length | 15.8 m |

We employ technology levels estimated for an entry into service of 2035, and use the values given in Table 1 following the analysis in our previous work [1]. The *conservative* level assumes incremental improvements on current technologies with no significant breakthroughs. The *optimistic* level assumes a significant breakthrough in battery technology, such as the commercialization of lithium-air batteries, and significant improvements in electrical machine and power electronics. A third level, the *intermediate* set, is added in between the conservative and optimistic values. Note that all values for batteries are at battery pack level, and already account for the packaging efficiency of combining cells to form packs.

### C. Baseline Aircraft and Calibration

Since our previous, cruise-only, study [1] identified small aircraft as the most likely to benefit from electrification, we select here what we refer to as a *commuter* aircraft as the conventional baseline reference. Specifically, our baseline is modeled after the Series 400 Twin Otter (originally manufactured by de Havilland Canada, now by Viking Air), whose major characteristics are summarized in Table 2.

In this section, the framework is calibrated to match the fuel burn of this baseline aircraft. Additionally, since the Twin Otter was designed in the 1960's, we model an *advanced technology* version of the baseline, and use this version as a basis for comparison of electrified aircraft. The assumptions made for the advanced technology baseline are: 20% reduction in engine core power specific fuel consumption, 20% reduction in turbine core mass (for a given power output) and 15% reduction in aircraft empty mass. These changes are based on the recommendations given by Raymer [8].

For all aircraft analyzed in this work (baseline, conventional, electrified), we impose a maximum take-off and landing distance of 1 000 m, and set lift coefficient and rate-of-climb values as given in Table 3. It should be noted that the Twin Otter is capable of using much shorter runways, but we adopt here a less-constraining field lengths that is still short enough to include most regional airports. Note also that this work focuses on relative changes due to electrification, and the exact value of the field length constraint is not such an important consideration as the technology level parameters are.

In order to ensure the accuracy of the comparisons made in the current work, the performance of the baseline conventional aircraft was calibrated with known data for the Twin Otter by adjusting the gas turbine power specific fuel

**Table 3 Performance constraints and related parameters used in the current work.**

| Parameter | Value |
|---|---|
| Takeoff and landing distances, $\ell_{\text{TO}}$ and $\ell_{\text{L}}$ | 1 000 m |
| Maximum lift coefficient $C_{L,\max}$ | 2.37[a] |
| Maximum rate of climb (ROC) | 8.13 m/s |

[a]Numerical value obtained from Torenbeek [20], and represents $C_{L,\max}$ in landing configuration. $C_{L,\max}$ during takeoff configuration taken as $0.82C_{L,\max,land}$, as also recommended in [20].

**Table 4 Baseline commuter aircraft results compared with manufacturer data [21] for the maximum range full fuel mission. The specific energy consumption is calibrated to match the manufacturer fuel burn.**

| | | Manufacturer | Calculated | Difference |
|---|---|---|---|---|
| Takeoff mass | [kg] | 5670 | 5305 | −6.4 % |
| Empty mass | [kg] | 3377 | 3109 | −7.9 % |
| Fuel burn (calibrated) | [kg] | 1164 | 1164 | - |
| Wing planform area | [$m^2$] | 39 | 46 | +18 % |

consumption (*PSFC*) in our framework so that the *PSEC* of the modeled aircraft matches exactly that of the baseline. This calibration is done for the maximum range full fuel mission for which all required performance data (takeoff mass, fuel mass, payload mass, mission range and reserve mission) are available from the Twin Otter's "Technical Specifications and Standard Equipment List" [21]. This longer mission has a range of $R_{\text{mis}}$ =1300 km (702 nmi) with cruising speed of 93.6 m/s (182 kts) and altitude of 3 048 m (10 000 ft), and a reserve requirement of 45 minutes flight time at cruise altitude and speed for maximum range. A climb and descent speed of 2.54 m/s (500 ft/min) is assumed. The cruise distance is automatically calculated so that the sum of the climb, cruise and descent segments match exactly the required mission range $R_{\text{mis}}$. The mission payload is 1 030 kg (2 270 lb), and the aircraft consumes 1 419 liters of fuel whose mass is 1 077 kg at an assumed density of 0.82 kg/liter for Jet A-1 fuel.

Table 4 shows some of the resulting data for the calibrated commuter aircraft performing this maximum range full fuel mission, compared to the results published by the manufacturer. All parameters predicted by the framework fall within 10% of the manufacturer values, except for the wing area. It is difficult to know which design constraint actually set the wing area requirement when the Twin Otter was designed, so with the takeoff and empty masses showing good agreement and the fuel burn calibrated to the baseline aircraft, the model is considered accurate enough for the level of fidelity of the models in the current work.

For the remaining of the present study, we use the more commonly flown *design mission* with a range of 463 km (250 nmi) and a payload capacity of 1 735 kg (17 passengers at 102 kg each, including luggage). Additionally the advanced technology baseline version is used for comparison with electrified aircraft given their assumed 2035 entry into service.

The sizing and performance results of the current and advanced technology baselines, both sized for the *design mission*, are given in Table 5. The predicted improvements in the engine and structure of the advanced technology baseline get compounded in the sizing process and results in a predicted 25% reduction in fuel burn. By comparing the electrified aircraft to this advanced baseline, any improvements in performance can be attributed directly to electrification.

### D. Electrification Design Space

By evaluating the model for a range of $f_S$ and $f_L$ values, a contour of the electrification design space can be created. When creating continuous sweeps over the design space, assumptions need to be made to ensure that each point represents a physically meaningful aircraft. In this case, it is assumed that both the amount of boundary layer ingested and the propulsor nacelle wetted surface (and thus weight and drag) scale with either $f_L$ or $(1 - f_L)$. The electrical propulsor components are scaled by $f_L$, and the mechanical propulsor components by $(1 - f_L)$. This assumption is

**Table 5 Comparison of current and advanced technology baseline aircraft for design mission of 463 km (250 nmi) range and 1 735 kg payload. PSEC is calculated assuming a specific energy of fuel of 43 MJ/kg.**

| | | Current Technology | Advanced Technology | Difference |
|---|---|---|---|---|
| Takeoff mass $M_{TO}$ | [kg] | 5146 | 4373 | −15 % |
| Empty mass $M_E$ | [kg] | 2914 | 2267 | −22 % |
| Fuel mass $M_{\text{fuel}}$ | [kg] | 497 | 371 | −25 % |
| Energy consumption $PSEC$ | [-] | 1.65 | 1.22 | −25 % |

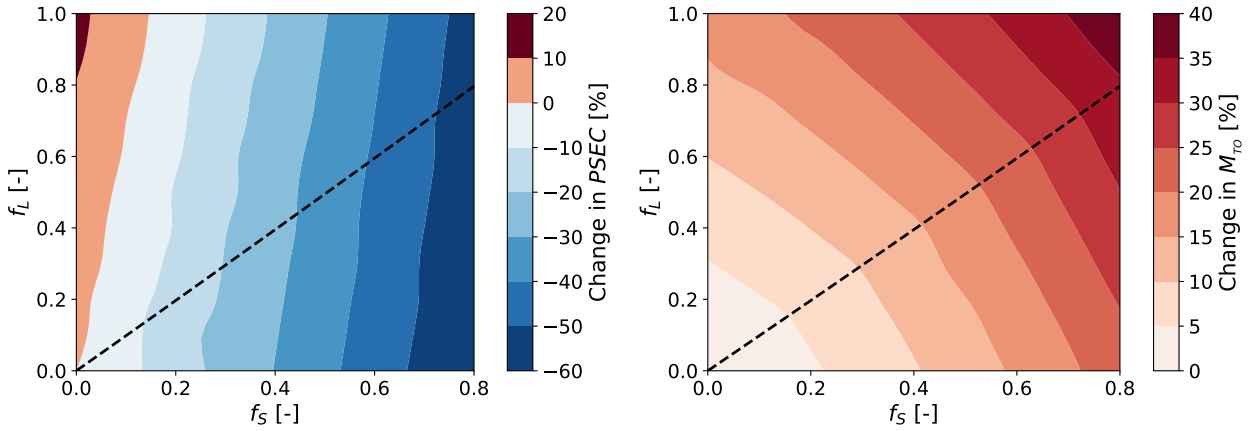


**Fig. 5 Percentage change in $PSEC$ (left) and $M_{TO}$ (right) as electrification is varied. Region below dashed line is parallel hybrid and region above is series. Results are shown for optimistic electrical technology assumptions.**

made to ensure that for the edge cases ($f_L = 0$ and $f_L = 1$), the unused propulsors physically disappear. For example, propulsors that provide 50% of the total power will be twice as big (in terms of physical dimensions) as ones providing 25% of the total power. However, at the edges, the assumptions are exact. For example, for $f_L = 0$, there are no electrical propulsors. A linear scaling such as this is likely a simplification, but it will still provide more realistic results compared to not scaling the propulsors at all.

For the conservative electrical technology assumptions (see Table 1), none of the aircraft in the design space lead to an improvement in $PSEC$. Thus, the results presented here assume the optimistic technology values. A contour plot of the $f_S$-$f_L$ design space for this set of assumptions is shown in Fig. 5. Note that the contours show the percentage change in $PSEC$ and $M_{TO}$ relative to the advanced baseline conventional aircraft, sized for the same mission. For the results shown here, it is assumed that the mechanical propulsors are two turbo-prop engines with 3-blade, 2.6 m diameter propellers, similar to the baseline Twin Otter. The electrical propulsors are assumed to be an array of 30 ducted fans, each with 0.35 m diameter that are integrated into the upper surface trailing edge of the wing. As will be explained in Section IV.E, this arrangement of electrical propulsors led to the highest $PSEC$ benefit for the all-electric case, and was thus used here.

Note that the design space is only shown for $f_S < 0.8$. This is because the region $f_S = 1, 0 \leq f_L < 1$ represents a non-physical boundary where all the power comes from a battery, and there is thus no way to power the mechanical propulsors. Because of this non-physicality, numerical issues start at $f_S \sim 0.8$. The notable exception is, of course, the all-electric case with $f_S = f_L = 1$.

Figure 5 shows that $PSEC$ changes much more rapidly as $f_S$ is increased compared to changes in $f_L$. This seems to indicate that the decision between parallel hybrid ($0 \leq f_S \leq 0.8$, $f_L = 0$), and series hybrid ($0 \leq f_S \leq 0.8$, $f_L = 1$) is not nearly as important as the decision between the power split between batteries and the gas turbine, as given by $f_S$. That being said, parallel hybrids are seen to be slightly more efficient than series ones. This can be attributed to the interaction of various phenomena. Firstly, the array of electrical propulsors have a lower overall propulsive area, which means it will have a lower propulsive efficiency for providing a given amount of power. This decrease in area is due to

**Table 6 All-electric performance with optimistic technology assumptions, under various levels of electrification. $PSEC$ and $M_{TO}$ change measured against the advanced technology baseline with $M_{TO}$ = 4373 kg and $PSEC$ = 1.22.**

| Case | Number of fans [-] | Fan diameters [m] | Battery mass [kg] | $M_{TO}$ change [%] | $PSEC$ change [%] |
|---|---|---|---|---|---|
| *a* | 2 | 2.6 | 2463 | +65 | -61 |
| *b* | 4 | 1.0 | 2258 | +45 | -65 |
| *c* | 20 | 0.53 | 2029 | +44 | -68 |
| *d* | 30 | 0.35 | 1987 | +41 | -69 |
| *e* | 40 | 0.26 | 1996 | +40 | -69 |
| *f* | 80 | 0.13 | 2153 | +43 | -69 |

the quadratic relationship between a propulsors area and its diameter. This implies that if a propulsor's diameter is halved, four such propulsors are needed to provide the same area as the original. In this case, the propulsors are spread out over the trailing edge of the wing. The resulting propulsors are of much smaller diameter, and their overall area is significantly less, despite there being thirty of them. Secondly, although this array of electrical propulsors have less propulsive area, they enable a significant amount of BLI. It is assumed here that 80% of the wing span (excluding the fuselage diameter), is covered with propulsors. Using Equation 17 from Section II.B, it can be estimated that the cases shown here with $f_L = 1$ ingest 32% of the total aircraft boundary layer. As per the $f_L$ scaling mentioned earlier, the amount of BLI then decreases linearly to zero as $f_L = 0$ is approached. For a parallel system, there are fewer components in the power conversion chain, making it inherently more efficient than a series system, where all the power from a gas turbine has to be converted via a generator. Lastly, because the overall propulsive area of the electrical propulsors are less, the total propulsor mass ends up being significantly less than that of two large propulsors. Overall, the net effect of all these factors is still a reduction in $PSEC$ for parallel configurations.

As $f_S$ increases, it can be seen that $PSEC$ decreases significantly, reaching a maximum reduction relative to the baseline conventional aircraft of up to 60%, albeit with a gain in $M_{TO}$ of up to 40%. This mass gain is primarily due to the battery at high $f_S$.

### E. All-Electric

The results from the previous section highlight the fact that $PSEC$ can only be decreased by increasing $f_S$. Furthermore, it was found that the all-electric case leads to the highest $PSEC$ benefit, and will thus be considered separately here. The individual effects of distributed propulsion (DP) and boundary layer ingestion (BLI) will also be investigated here. An all-electric model using the conservative electrical technology assumptions was found not to close. Only the optimistic assumptions will thus be used here.

Various different levels of BLI and distribution were investigated under different strategies of propulsor sizing. For case *(a)*, the propulsive area of the turboprop propellers are kept constant, thus resulting in two very large ducted fans (2.6 m in diameter). Since these represent unrealistically large ducted propulsors for an aircraft of this size, case *(b)* considers two more reasonably sized 1 m diameter ducted fans. For cases *(c-f)*, 20, 30, 40 and 80 fans were distributed over the wing to investigate the effects of massively distributing the propulsors. As in Section IV.D, the diameters of these fans were calculated to cover 80% of the upper wing surface, and thus ingest 32% of the total aircraft boundary layer.

Table 6 shows the outcome of this investigation. All-electric aircraft have the potential of leading to significant reductions in PSEC, at the expense of higher takeoff mass, mainly due to the large battery mass. Interestingly, both battery and thus takeoff mas vary significantly for different degrees of distribution, whereas $PSEC$ reaches a plateau at around 30 propulsors,which also coincides with the point of minimum battery mass and is near the point of minimum takeoff mass. The trends observed can be explained as follows: for case *(a)*, the takeoff mass is high because of the very large ducted fans, which are heavy and cause a lot of dissipation (drag). For case *(b)*, the fans are more realistically sized, but the propulsive area is much smaller and a larger air mass has to be accelerated to power the aircraft, leading to a lower propulsive efficiency. For cases *(c-f)*, as the number of propulsors increases, their total mass decreases, as does the total propulsive area, because of the quadratic relationship between fan diameter and area.

Initially, the decrease in mass outweighs the decrease in propulsive efficiency, but after 30 fans, the loss in propulsive efficiency becomes detrimental, leading to an optimum number of fans of around $30 \times 0.35$ m diameter fans. This was

**Table 7 Extended range hybrid-electric performance. $PSEC$ and $M_{TO}$ change measured against advanced technology baseline with $M_{TO}$ = 4852 kg and $PSEC$ = 1.36 for baseline conventional.**

| Configuration | Tech assump. | Climb $f_S$ [-] | Cruise $f_S$ [-] | $M_{TO}$ change [%] | $PSEC$ change [%] |
|---|---|---|---|---|---|
| Baseline conventional | N/A | 0 | 0 | - | - |
| Fixed hybrid | Conservative | 0.2 | 0.2 | +48 | +1.5 |
| | Intermediate | 0.55 | 0.55 | +59 | -27 |
| | Optimistic | 0.9 | 0.9 | +52 | -63 |
| Varying hybrid | Conservative | - | - | - | - |
| | Intermediate | - | - | - | - |
| | Optimistic | 1 | 0 | +15 | -3.7 |

the motivation for using 30 fans in the design space exploration of Section IV.D. The aircraft with 30 fans has the lowest battery mass, nearly the lowest gain in $M_{TO}$, and is the point where increasing fan count does not lead to a further reduction in $PSEC$. Nevertheless, all versions considered provide a significant reduction in $PSEC$, and even though their masses also grow significantly, the concepts still seem promising, given the high energy savings. Furthermore, the all-electric, under the optimistic technology assumptions can still efficiently ($PSEC$ = 0.46) perform missions of up to 740 km (400 nmi). Beyond that point, however, performance constraints become active and the design becomes infeasible. At that point, the battery accounts for just under half of the total aircraft mass.

### F. Hybrid-Electric

Since it was shown in Section IV.D that the parallel hybrid configuration is in general more efficient than the series, only the parallel case will be investigated here. The hybrid-electric configuration provides the opportunity to reap the benefits of the high efficiency of the battery system, while allowing higher ranges to be feasible. It is therefore instructive to look at a higher-range mission than the design mission. An *extended range* mission with $R_{\text{mis}}$ = 926 km (500 nmi) is thus considered.

In the previous sections, it was assumed that $f_S$ and $f_L$ remain fixed at one value throughout the mission. In this section, *electrification strategies* that vary by flight segment are also considered, where different segments can have different $f_S$ and $f_L$ values. Note that every propulsion subsystem component is sized for the maximum power that could be seen throughout the mission for all cases considered here. Such an electrification strategy that varies by segment thus allows for different propulsion subsystems to be sized for different conditions, thus potentially leading to some system-level benefits.

Additionally, an *intermediate* electrical technology level assumption is introduced here to look at the case of technology improving by more than just incremental steps to reach the conservative assumptions level, but not quite by the step changes assumed for the optimistic assumptions. These values are also listed in Table 1. For each of the technology levels, two cases are considered: first, where electrification level ($f_S$, $f_L$) is constant during the mission, or *fixed hybrid*; and second, where the climb segment has a different electrification level than cruise (with the electrification of the descent segment fixed to that of the cruise).

Table 7 summarizes the outcome of these studies. For the case of the fixed hybrid, it can be seen that both intermediate and optimistic technology levels predict significant reductions in $PSEC$: 27% and 63% respectively. In contrast, this configuration does not provide a benefit for the conservative assumptions. The predicted reductions for the former cases, however, come at the cost of a roughly 50% gain in $M_{TO}$. These results indicate that hybrid configurations provide a good solution to achieving high efficiencies at mission ranges that cannot be performed with an all-electric configuration. For the case of the hybrids with different climb and cruise electrification levels, it was found that only the optimistic technology level leads to a reduction in $PSEC$. This reduction is also very modest compared to that for the fixed hybrids. The expected benefits of sizing the electrical propulsor components for the high-power climb segment and the conventional components for the cruise, thus end up being minimal or non-existent.

## V. Summary and Conclusions

In this paper, a sizing and optimization framework that can be used to model aircraft with varying degrees of electrification was presented. This framework can also be used to model aircraft of significantly different sizes. Because of these capabilities, the framework is perfectly suited to explore the large design space associated with electrified aircraft.

Expanding on our previous work [1], the framework was used here to explore the propulsion system design space of a commuter aircraft Whereas the previous study only looked at a cruise segment and sized the aircraft for this single design point, the current work significantly improves the fidelity of the analyses by modeling the entire mission, including climb, cruise and descent segments, as well as a reserve mission. The propulsion system is then sized for the maximum power that it requires both to perform the mission and to meet various performance constraints.

Additionally, a *unified* propulsion system model that models electrification based on the source power split between a battery and a turbine and the load power split between electrically and mechanically powered fans (or propellers) is presented. Using this two-variable parameterization, the entire design space of propulsion system architectures, from conventional to all-electric, hybrid-electric and turbo-electric, can be modeled.

This design space was then explored for a commuter aircraft, carrying up to 19 passengers relatively short distances. A *design* mission with a range of 463 km (250 nmi) and an *extended range* mission with a range of 926 km (500 nmi) were considered. Different electrical technology level assumptions were also explored, assuming entry into service around the 2035 time frame. The Viking DHC-6 Twin Otter was modeled as a representative baseline aircraft, and this model was calibrated using manufacturer data to exactly predict the fuel burn of the real aircraft. An *advanced technology* version of this aircraft was then created to serve as a basis for comparison of the electrified aircraft.

Under the conservative electrical technology assumptions, it was found that an *all-electric* aircraft of this class is not feasible for the design mission, and even if the range is reduced significantly, the design does not close since the reserve requirements alone require a substantial amount of energy. Additionally, it was found that neither hybrid- nor turbo-electric configurations could result in a reduction in energy usage.

When considering the optimistic technology assumptions, the conclusions for the *all-electric* case are very different: such a configuration could lead to a 69% reduction in energy usage for the design mission, compared to the conventional baseline. The extended range mission was, however, beyond its feasible range. This reduction in energy assumes a significant degree of distribution of the propulsors, with 30 small electric propulsors embedded in the upper wing surface trailing edge, allowing for up to 32% of the total aircraft momentum defect to be ingested. Without the large degree of distribution and boundary layer ingestion (BLI), the aircraft still sees a 63% reduction in energy usage, where 3% of the additional benefit is due to distribution and a further 3% to BLI. These high levels of benefit, however, come at the cost of a takeoff mass increase of around 50%.

For the optimistic technology assumption, it was found that a *hybrid-electric* configuration could enable much longer missions to be performed than the all-electric. By using primarily battery energy and a relatively small amount of fuel, the extended range mission could be performed with a 63% reduction in energy usage, compared to a conventional aircraft also sized for the longer mission. This significant improvement, however, comes at the cost of a 52% increase in takeoff mass, mainly due to the battery. For the hybrid case, a (perhaps more realistic) intermediate technology level was also considered and it was found that under those assumptions a 29% reduction in energy requirement might be realized, although also at a growth in takeoff mass of 55%. It was found that parallel hybrid architectures are in general slightly more efficient than series ones.

Lastly, the effects of implementing electrification schemes that vary by flight segment were investigated. It was found that even though this might lead to more efficient subsystem sizing, where the electrical system is sized for the climb segment, and the conventional subsystem for cruise, the net effect is either an increase in energy usage or a very slight decrease on the order of only a few few percent, compared to the 63% and 52% mentioned above, depending on technology level.

In conclusion, it can be stated that the potential benefits of the electrification of commuter aircraft depend strongly on the electrical component technology levels assumed; in particular the battery specific energy. If technology levels stay near today's state of the art, it is unlikely that such aircraft would prove to be beneficial. However, if technology levels increase significantly, all-electric configurations could lead to substantial energy usage reductions. Here, a 69% reduction was estimated, albeit it for relatively short range missions. Hybrid-electric configurations, however, could allow for much longer range missions to be flown, while experiencing much of the energy usage benefits seen by all-electric configurations. Here, a benefit of 63% was estimated for the optimistic technology level assumptions, and a 27% benefit for intermediate levels. Technologies such as distributed propulsion and boundary layer ingestion also show

definite system-level benefits, and leveraging them efficiently could prove to be a key area of innovation when electric propulsion systems are more widely implemented in aircraft.

## References


[1] Kruger, M., Byahut, S., Uranga, A., Dowdle, A., Gonzalez, J., and Hall, D. K., "Electrified Aircraft Trade-Space Exploration," AIAA 2018-4227, 2018 AIAA Aviation, Atlanta, GA, 25–29 June, 2018. https://doi.org/10.2514/6.2018-4227.

[2] Welstead, J., and Felder, J., "Conceptual Design of a Single-Aisle Turboelectric Commercial Transport with Fuselage Boundary Layer Ingestion," AIAA 2016-1027, 2016 AIAA SciTech, San Diego, CA, 4–8 January, 2016. https://doi.org/10.2514/6.2016-1028.

[3] Antcliff, K., Guynn, M., T.V, M., Wells, D., Schneider, S., and Tong, M., "Mission Analysis and Aircraft Sizing of a Hybrid-Electric Regional Aircraft," AIAA 2016-1028, 2016 AIAA SciTech, San Diego, CA, 4–8 January, 2016. https://doi.org/10.2514/6.2016-1027.

[4] Isikveren, A. T., Pornet, C., Vratny, P. C., and Schmidt, M., "Optimization of Commercial Aircraft Using Battery-Based Voltaic-Joule/Brayton Propulsion," *Journal of Aircraft*, 2016. https://doi.org/10.2514/1.C033885.

[5] Bradley, M., and Dorney, C., "Subsonic Ultra Green Aircraft Research: Phase II – Volume II – Hybrid Electric Design Exploration," 2015.

[6] Lukaczyk, T. W., Wendorff, A. D., Colonno, M., Economon, T. D., Alonso, J. J., Orra, T. H., and Ilario, C., "SUAVE: An Open-Source Environment for Multi-Fidelity Conceptual Vehicle Design," AIAA 2015-3087, 2015 AIAA Aviation, Dallas, TX, 22–26 June, 2015. https://doi.org/10.2514/6.2015-3087.

[7] Perez, R. E., Jansen, P. W., and Martins, J. R. R. A., "pyOpt: A Python-Based Object-Oriented Framework for Nonlinear Constrained Optimization," *Structural and Multidisciplinary Optimization*, Vol. 45, No. 1, 2012, pp. 101–118. https://doi.org/10.1007/s00158-011-0666-3.

[8] Raymer, D., *Aircraft Design: A Conceptual Approach*, 5$^{th}$ ed., American Institute of Aeronautics & Astronautics, 2012.

[9] Torenbeek, E., *Synthesis of Subsonic Airplane Design*, Springer Science & Business Media, 2013.

[10] Waters, M. H., and Schairer, E. T., "Analysis of Turbofan Propulsion System Weight and Dimensions," Tech. rep., NASA Ames Research Center, 1977.

[11] Wick, A. T., Hooker, J. R., and Zeune, C. H., "Integrated Aerodynamic Benefits of Distributed Propulsion," AIAA 2015-1500, 2015 AIAA SciTech, Kissimmee, FL, 5–9 January, 2015. https://doi.org/10.2514/6.2015-1500.

[12] Drela, M., *Flight Vehicle Aerodynamics*, MIT Press, 2014.

[13] Drela, M., "Power Balance in Aerodynamic Flows," *AIAA Journal*, Vol. 47, No. 7, 2009, p. 1761. https://doi.org/10.2514/1.42409.

[14] Hall, D. K., Huang, A. C., Uranga, A., Greitzer, E. M., Drela, M., and Sato, S., "Boundary Layer Ingestion Propulsion Benefit for Transport Aircraft," *Journal of Propulsion and Power*, Vol. 33, No. 5, 2017, pp. 1118–1129. https://doi.org/10.2514/1.B36321.

[15] Uranga, A., Drela, M., Hall, D. K., and Greitzer, E. M., "Analysis of the Aerodynamic Benefit from Boundary Layer Ingestion for Transport Aircraft," *AIAA Journal*, Vol. 56, No. 11, 2018, pp. 4271–4281. https://doi.org/10.2514/1.J056781.

[16] Gill, P. E., Murray, W., and Saunders, M. A., "SNOPT: An SQP Algorithm for Large-Scale Constrained Optimization," *SIAM Review*, Vol. 47, 2005, pp. 99–131. https://doi.org/10.1137/S0036144504446096.

[17] Botero, E. M., Wendorff, A., MacDonald, T., Variyar, A., Vegh, J. M., Lukaczyk, T. W., Alonso, J. J., Orra, T. H., and Ilario da Silva, C., "SUAVE: An Open-Source Environment for Conceptual Vehicle Design and Optimization," AIAA 2016-1275, 2016 AIAA SciTech, San Diego, CA, 4–8 January, 2016. https://doi.org/10.2514/6.2016-1275.

[18] Wendorff, A., Botero, E., and Alonso, J. J., "Comparing Different Off-the-Shelf Optimizers' Performance in Conceptual Aircraft Design," AIAA 2016-3362, 2016 AIAA Aviation, Washington, DC, 13–17 June, 2016. https://doi.org/10.2514/6.2016-3362.

[19] Kroo, I., Altus, S., Braun, R., Gage, P., and Sobieski, I., "Multidisciplinary Optimization Methods for Aircraft Preliminary Design," AIAA 1994-4325, Symposium on Multidisciplinary Analysis and Optimization, Panama City Beach, FL, 7–9 September, 1994. https://doi.org/10.2514/6.1994-4325.

[20] Torenbeek, E., *Advanced Aircraft Design: Conceptual Design, Technology and Optimization of Subsonic Civil Airplanes*, John Wiley & Sons, 2013.

[21] Viking Air Ltd., "Viking Twin Otter Series 400 Technical Specifications and Standard Equipment List," , 2016.